Fluid and Particle Coarsening of Drag Force for Discrete-Parcel Approach

Article · August 2016

DOI: 10.1016/j.ces.2016.08.014

4 authors:

Ali Ozel

Princeton University

18 PUBLICATIONS **43** CITATIONS

SEE PROFILE

Jari Kolehmainen

Princeton University

10 PUBLICATIONS **8** CITATIONS

SEE PROFILE

Stefan Radl

Graz University of Technology

89 PUBLICATIONS **368** CITATIONS

SEE PROFILE

Sankaran Sundaresan

Princeton University

226 PUBLICATIONS **5,237** CITATIONS

SEE PROFILE

Fluid and Particle Coarsening of Drag Force for Discrete-Parcel Approach

Ali Ozel, Jari Kolehmainen, Stefan Radl, Sankaran Sundaresan

Chemical Engineering Science

www.elsevier.com/locate/ces

PII: S0009-2509(16)30436-5
DOI: http://dx.doi.org/10.1016/j.ces.2016.08.014
Reference: CES13111

To appear in: *Chemical Engineering Science*

Received date: 9 June 2016
Revised date: 2 August 2016
Accepted date: 8 August 2016

Cite this article as: Ali Ozel, Jari Kolehmainen, Stefan Radl and Sankaran Sundaresan, Fluid and Particle Coarsening of Drag Force for Discrete-Parcel Approach, *Chemical Engineering Science* http://dx.doi.org/10.1016/j.ces.2016.08.014

Fluid and Particle Coarsening of Drag Force for Discrete-Parcel Approach

Ali Ozel[a,*], Jari Kolehmainen[a], Stefan Radl[b], Sankaran Sundaresan[a]

[a] *Department of Chemical and Biological Engineering, Princeton University, Princeton, NJ 08544, USA*
[b] *Institute of Process and Particle Engineering, Graz University of Technology, Inffeldgasse 13/III, 8010 Graz, Austria*

Abstract

Fine-grid Euler-Lagrange simulations of gas-fluidization of uniformly sized particles have been performed in three-dimensional periodic domains. Snapshots obtained from these simulations have been systematically coarse-grained to extract filter size dependent corrections to the drag law that should be employed in coarse Euler-Euler (EE) simulations. Correction to the drag law that should be employed in Coarse Multi-Phase Particle-in-Cell (MP-PIC) model simulations is examined through a two-step process: separating the coarsening of the fluid and particle phases. It is found that the drag correction is almost entirely due to the coarsening of the fluid cells, with particle coarsening having only a weak effect. It is shown that drag correction for coarse EE and MP-PIC simulations are comparable. As a result, coarse drag models developed for EE simulations can serve as a good estimate for corrections in MP-PIC simulations, and vice versa.

Keywords: MP-PIC, parcel approach, fluid coarsening, particle coarsening, drag force, filtered two-fluid model

1. Introduction

Industrial-scale gas-particle flow systems exhibit flow structures which span a wide range of spatial and temporal scales; bubble-like voids of varying sizes rising at different velocities form in dense beds, while dynamic clusters of different shapes and sizes are found in dilute flows. These meso-scale structures affect the macro-scale flow patterns, which impacts the performance of fluidized bed chemical reactors. This multi-scale nature of flow complicates analysis and scale-up of these devices. Coarse simulation methods that can reproduce reliably the macro-scale flow structures in these devices have been a topic of much research (Agrawal et al., 2001; Wang and Li, 2007; Igci and Sundaresan, 2011a; Parmentier et al., 2012; Ozel et al., 2013; Milioli et al., 2013; Schneiderbauer and Pirker, 2014).

Industrial-scale fluidized bed simulations can be classified into two groups: (1) Eulerian-Eulerian simulations based on two-fluid model (TFM) approach (Gidaspow, 1994; Syamlal et al., 1993; Balzer et al., 1998) and (2) Eulerian-Lagrangian simulations based on multiphase particle-in-cell method (MP-PIC) (Snider, 2001; Snider and Banerjee, 2010; Snider et al., 2011).

*Corresponding author
Email address: aozel@princeton.edu (Ali Ozel)

In TFM simulations of gas-particle flows, one must postulate models for the interphase interaction force and the effective stresses in the two phases. The particle phase stress model is either postulated in an ad-hoc manner (Jackson, 2000) or calculated using the kinetic theory for granular flow (KTGF) and a fluctuating granular energy equation (e.g., see Gidaspow (1994); Koch and Sangani (1999); Balzer et al. (1998); Lun et al. (1984); Ding and Gidaspow (1990)). In MP-PIC simulations, the continuum averaged equations of motion for the gas phase are solved on an Eulerian grid, while representative particles, commonly referred to as parcels representing a plurality of real particles, are tracked in a Lagrangian manner. As in TFM, this approach requires a model for the interphase interaction force. Furthermore, collisions between parcels are not tracked; but are captured indirectly through a postulated particle phase stress (Snider, 2001; O'Rourke and Snider, 2012; O'Rourke et al., 2009; Snider, 2007). The Discrete Particle Model (DPM) proposed by Patankar and Joseph (2001) seeks to circumvent the need for postulating a stress model in the parcel-based simulation by treating the parcels as effectively larger particles and tracking collisions between the parcels. Collision tracking is generally very expensive and hence DPM-based approach has not gained much attraction for industrial scale device simulations.

It is generally accepted that meso-scale structures affect the macro-scale flow characteristics. As a result, one must either resolve the meso-scale structures or recognize their consequences in some indirect manner. Li and Kwauk (1994) recognized that the presence of clusters leads to a significant decrease in the effective fluid-particle drag and introduced the energy-minimization-multi-scale (EMMS) method, which has been refined and extended since then (Wang and Li, 2007; Wang et al., 2008). The meso-scale patterns, which the EMMS method sought to average over, can be observed in TFM simulations when fine numerical grids are employed (e.g., see Agrawal et al. (2001); Ozel et al. (2013)). MP-PIC simulations with fine grids reveal these structures as well; indeed, with fine Eulerian grids, both TFM and MP-PIC approaches reveal similar meso-scale structures (Benyahia and Sundaresan, 2012).

When fine numerical grids are employed, all the particles are tracked in an Euler-Lagrange simulation (i.e. parcel size is one), and all the collisions are resolved, one obtains the so-called Computational Fluid Dynamics-Discrete Element Method (CFD-DEM). This method has served as a vehicle to probe meso-scale flow structures (Ye et al., 2004; Capecelatro and Desjardins, 2013; Capecelatro et al., 2014a,b; Radl and Sundaresan, 2014; Salikov et al., 2015) and the consequences of complex particle-particle interactions (Kobayashi et al., 2013; Girardi et al., 2016; Kolehmainen et al., 2016; Gu et al., 2016; Fries et al., 2013). The CFD-DEM approach is computationally expensive and is limited to small-scale flows, as one can realistically track no more than a few million particles.

The use of fine grids is not practical for industrial scale flow problems (Sundaresan, 2000), necessitating the use of coarse (fluid) grids in both TFM and MP-PIC methods and treatment of particle-particle interactions through a stress model. Such coarse simulations require coarse-grained constitutive models to account for the consequences of unresolved flow structures.

A procedure for systematically coarse-graining the TFM to obtain the so-called filtered TFM has already

been presented in the literature (Igci et al., 2008; Parmentier et al., 2012; Ozel et al., 2013; Milioli et al., 2013; Schneiderbauer and Pirker, 2014; O'Brien, 2014; Fox, 2014) The filtered TFM contains additional residual correlations (such as filtered solid stress and drag force), which must be modeled. It is now known that the filtered drag force depends on filter size and can be significantly smaller than that predicted by the original drag force models; this correction to the drag law is the most important difference between the original and filtered TFMs (Igci and Sundaresan, 2011a; Parmentier et al., 2012; Ozel et al., 2013; Milioli et al., 2013; Schneiderbauer and Pirker, 2014). Ozarkar et al. (2015) show that the sub-grid contribution of particle phase stress has a slight effect on the macroscopic flow predictions such as time-average pressure and velocity profiles, as well as the solids inventory in a dense fluidized bed. However, in the context of dilute dispersed flows, Moreau et al. (2009) point out that the trace of sub-grid contribution of particle stresses has a dispersive characteristic and it is crucial to obtaining a better prediction of particle segregation.

Coarse-graining CFD-DEM simulation results is beginning to gain attention only recently (Radl and Sundaresan, 2014; Capecelatro et al., 2014b,a, 2016b,a), motivated by the need for closures to be used in coarser models. These authors have simulated fluidized suspensions in fully/wall-bounded periodic domains and analyzed the snapshots. Radl and Sundaresan (2014) examined how the drag law should be modified when one coarsens the fluid grid size, while continuing to simulate through DEM the motion of all the particles in the simulation domain. Such coarsening, referred to as *fluid coarsening*, revealed the need for a filter size dependent effective drag law, which is conceptually similar to what is known in the context of TFMs. These authors speculated that the drag law may also depend on parcel size in both MP-PIC and DPM based approaches. However, they did not perform a systematic *particle coarsening* to check whether their speculation is correct, or considered the derivation of drag closures for Euler-Euler-based models from their CFD-DEM data. In contrast, Capecelatro et al. (2016b,a) propose closures for Reynolds-averaged Euler-Euler-based models for gas-particle flows from CFD-DEM predictions. It should be remarked that there is a long history of seeking closures for effective stresses and fluid turbulence particle interactions in Euler-Euler models from Euler-Lagrange simulation results (e.g., see Simonin (1991); Vance et al. (2006); Fede and Simonin (2006); Kaufmann et al. (2008)); however, these studies typically do not seek correction to drag.

The present study is concerned with a systematic coarsening of computational data generated through detailed simulations to develop effective drag force models for filtered Euler-Euler and MP-PIC approaches. Although it would be desirable to generate the required computational data through fully-resolved Euler-Lagrange simulations, where the motion of the particles are followed using Newton's equations and the interstitial fluid flow is completely resolved through direct numerical simulation (Koch and Ladd, 1997; Derksen and Sundaresan, 2007; Rubinstein et al., 2016; Tenneti et al., 2010, 2011; Vincent et al., 2014; Ozel et al., 2016), such simulations are very expensive and flows involving only a few thousand particles can realistically be simulated through this approach. In contrast, one can readily perform CFD-DEM simulations, which requires a microscopic drag law as an input, in larger domains containing millions of

particles (Capecelatro et al., 2014a). Hence, this approach is more suitable for developing filtered drag laws that are applicable for very coarse simulations. Work aimed at developing such coarse drag laws by filtering CFD-DEM simulation results are beginning to emerge (Radl and Sundaresan, 2014; Girardi et al., 2016; Capecelatro et al., 2016b,a).

One can also generate computational data through finely resolved Euler-Euler simulations, but these simulations require particle phase stress model as well. Continuum particle-phase stress models that account for complex particle-particle interactions, such as van der Waals, capillary or electrostatic interactions, are still under development. In contrast, these interactions are quite easily included in CFD-DEM simulations, and therefore we pursue CFD-DEM simulations to generate the computational database needed for coarse model development.

By filtering the CFD-DEM results, one can generate four types of results: (1) coarse-grained drag that can be used with filtered Euler-Euler simulations, (2) coarse-grained drag model that can be used with coarse MP-PIC and coarse CFD-DPM simulations, (3) continuum particle phase stress model that can be used in well resolved Euler-Euler simulations, and (4) coarse-grained stress models that can be used with filtered Euler-Euler and coarse MP-PIC simulations. In the present study, we are concerned with items 1 and 2 in the above list.

The general approach to extract such drag models is follows. In the CFD-DEM simulations used to generate the snapshots, a user-specified grid size is employed to solve the averaged equation for the gas phase, which is $3d_p$ in the examples presented in this paper, where d_p denotes particle diameter. In order to develop effective drag law for filtered Euler-Euler approach, we first map the Lagrangian variables from particle locations onto the Eulerian field and then compute the filtered Eulerian drag force for different filter sizes by following the procedure already outlined in the literature (Igci and Sundaresan, 2011a; Ozel et al., 2013). Drag model for Euler-Lagrange simulations can be coarsened in two ways: (1) One seeks modifications to the drag force model when only coarsening the grid size used for solving the fluid phase equations, while continuing to solve for the motion of all the particles as in the original fine-grid simulation. This is the *fluid coarsening* referred to earlier. (2) One seeks a modified drag law that applies when one further coarsens the problem by following the motion of only a subset of the particles (along with the fluid coarsening). This is the *particle coarsening* referred to earlier. This is illustrated in Figure 1 schematically. In general, particle coarsening should be accompanied by fluid coarsening as well, since one must have a fair number of representative particles inside each fluid cell to get reasonable statistics.

In the present study we address the following questions:

- What is the relative importance of fluid and particle coarsening on the extent of correction to the drag law for coarse Euler-Lagrange simulations?
- When applying the drag law, the drag force is evaluated in the Eulerian cell (i.e., in Euler-Euler based models) and at the particle (parcel) location in the other (when seeking to perform well resolved simulations, researchers currently use the same drag law (e.g., Wen and Yu (1966)) in both Euler-Euler

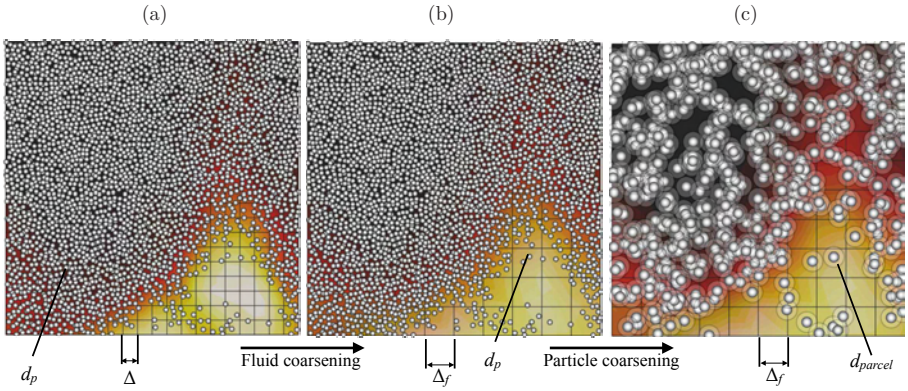

Figure 1: Schematic illustration showing fine-grid Euler-Lagrange simulations (panel (a); colors indicate the local particle concentration) to obtain constitutive relationships for fluid-coarsened (panel (b)), and coarse-grid MP-PIC simulations with parcels representative of many particles (panel (c), d_{parcel} refers to the diameter of a parcel).

and Euler-Lagrange simulations.) How does this difference affect the fashion in which the effective drag law changes with extent of coarsening for the Euler-Euler and Euler-Lagrange simulations?

To answer these questions, we coarse-grain the same set of computationally generated snapshots to extract effective drag corrections applicable to both coarse Euler-Euler and Euler-Lagrange simulations. We will demonstrate that fluid coarsening is mostly responsible for the correction to the drag law and that for small filter sizes there is a small difference in the coarsened drag laws for the Euler-Euler and Euler-Lagrange simulations. This difference becomes smaller as one increases the extent of fluid and particle coarsening. As a result, one can, to a good approximation, avail the drag corrections developed in the literature for coarse Euler-Euler simulations in coarse Euler-Lagrange simulations as well.

This paper is organized as follows. We present the mathematical modeling and flow configuration, which is a 3D fully periodic square prism, in §2. Fluid and particle coarsening procedures are described in §3. In §4, the coarse-grained results are presented. The principal results are summarized in section, §5.

2. Mathematical Modeling and Flow Configuration

In the Discrete Element Method (DEM) (Cundall and Strack, 1979), particles are tracked by solving Newton's equations of motion:

$$m_i \frac{d\boldsymbol{v}_i}{dt} = \sum_j (\boldsymbol{f}^n_{c,ij} + \boldsymbol{f}^t_{c,ij}) + \boldsymbol{f}_{g\to p,i} + m_i \boldsymbol{g} \tag{1}$$

$$I_i \frac{d\boldsymbol{\omega}_i}{dt} = \sum_j \boldsymbol{T}_{t,ij} \tag{2}$$

In the equations, particle i is spherical and has mass m_i, moment of inertia I_i, translational and angular velocities $\boldsymbol{v}_i$ and $\boldsymbol{\omega}_i$. The forces acting on the particle i are: $\boldsymbol{f}^n_{c,ij}$ and $\boldsymbol{f}^t_{c,ij}$ which are the normal and

tangential contact forces between two particles i and j; $\boldsymbol{f}_{g\to p,i}$ which is the total interaction force on the particle i due to surrounding gas (explained further below), and $m_i\boldsymbol{g}$ is the gravitational force. The torque acting on particle i due to particle j is $\boldsymbol{T}_{t,ij}$. $\boldsymbol{T}_{t,ij} = \boldsymbol{R}_{ij} \times \boldsymbol{f}^t_{c,ij}$, where $\boldsymbol{R}_{ij}$ is the vector from the center of particle i to the contact point.

The particle contact forces $\boldsymbol{f}^n_{c,ij}$ and $\boldsymbol{f}^t_{c,ij}$ are calculated by the following Johnson and Johnson (1987); Di Renzo and Di Maio (2004):

$$\boldsymbol{f}^n_{c,ij} = \frac{4}{3}Y^*\sqrt{r^*}\delta_n^{3/2}\boldsymbol{n}_{ij} + 2\sqrt{\frac{5}{6}}\beta\sqrt{S_n m^*}\boldsymbol{v}^n_{ij}, \tag{3}$$

$$\boldsymbol{f}^t_{c,ij} = \begin{cases} -8G^*\sqrt{r^*\delta_n}\boldsymbol{t}_{ij} + 2\sqrt{\frac{5}{6}}\beta\sqrt{S_t m^*}\boldsymbol{v}^t_{ij} & for \quad \left|\boldsymbol{f}^t_{c,ij}\right| < \mu_s\left|\boldsymbol{f}^n_{c,ij}\right| \\ -\mu_s\left|\boldsymbol{f}^n_{c,ij}\right|\frac{\boldsymbol{t}_{ij}}{|\boldsymbol{t}_{ij}|} & for \quad \left|\boldsymbol{f}^t_{c,ij}\right| \geq \mu_s\left|\boldsymbol{f}^n_{c,ij}\right|, \end{cases} \tag{4}$$

where

$$\frac{1}{Y^*} = \frac{1-\nu_i^2}{Y_i} + \frac{1-\nu_j^2}{Y_j}, \quad \frac{1}{r^*} = \frac{1}{r_i} + \frac{1}{r_j}, \tag{5}$$

$$\beta = \frac{ln(e)}{\sqrt{ln^2(e)+\pi^2}}, \quad S_n = 2Y^*\sqrt{r^*\delta_n}, \tag{6}$$

$$\frac{1}{G^*} = \frac{2(2+\nu_i)(1-\nu_i)}{Y_i} + \frac{2(2+\nu_j)(1-\nu_j)}{Y_j}, \quad S_t = 8G^*\sqrt{r^*\delta_n}. \tag{7}$$

The subscripts i, j denote spherical particle i or j, and the superscript $*$ denotes the effective particle property of those two particles. The effective particle mass m^* is calculated as $m^* = m_i m_j/(m_i+m_j)$; δ_n is normal overlap distance; $\boldsymbol{n}_{ij}$ represents the unit normal vector pointing from particle j to particle i; $\boldsymbol{v}^n_{ij}$ represents the normal velocity of particle j relative to particle i; $\boldsymbol{t}_{ij}$ represents the tangential displacement obtained from the integration of the relative tangential velocity during the contact, $\boldsymbol{v}^t_{ij}$; and μ_s is the particle sliding friction coefficient. Here, Y is Young's modulus, G is shear modulus, ν is Poisson's ratio, and r is particle radius.

The fluid phase is modeled by solving the following conservation of mass and momentum equations in terms of the locally averaged variables over a computational cell:

$$\frac{\partial}{\partial t}(1-\phi) + \boldsymbol{\nabla}\cdot[(1-\phi)\boldsymbol{u}_g] = 0, \tag{8}$$

$$\rho_g(1-\phi)\left(\frac{\partial \boldsymbol{u}_g}{\partial t} + \boldsymbol{u}_g\cdot\boldsymbol{\nabla}\boldsymbol{u}_g\right) = -\boldsymbol{\nabla}p_g + \boldsymbol{\nabla}\cdot\boldsymbol{\tau}_g + \boldsymbol{\Phi}_d + \rho_g(1-\phi)\boldsymbol{g}. \tag{9}$$

Here, ρ_g is the density of the gas which is assumed to be constant, ϕ is the solid volume fraction, $\boldsymbol{u}_g$ is the gas velocity, p_g is the gas phase pressure, $\boldsymbol{\tau}_g$ is the gas phase deviatoric stress tensor. The total gas-particle interaction force per unit volume of the mixture $-\boldsymbol{\Phi}_d$, exerted on the particles by the gas, is composed of a generalized buoyancy force due to the slowly-varying (in space) local-average gas phase stress $(-p_g\boldsymbol{I} + \boldsymbol{\tau}_g)$ and the force due to the rapidly varying flow (in space) field around the particles.

In finite volume method based computations employed in our simulations, $\mathbf{\Phi}_d$ in any computational cell is related to $\boldsymbol{f}_{g\rightarrow p,i}$ of all the particles in that cell as $\mathbf{\Phi}_d = -\frac{\sum_i^{cell} \boldsymbol{f}_{g\rightarrow p,i}}{V}$ where V is the volume of the computational cell. On a per particle basis, the total interaction force on the particle by the gas can be written as $\boldsymbol{f}_{g\rightarrow p,i} = -\mathcal{V}_{p,i}\boldsymbol{\nabla} p_g|_{\mathbf{x}=\mathbf{x}_{p,i}} + \mathcal{V}_{p,i}\boldsymbol{\nabla}\cdot\boldsymbol{\tau}_g|_{\mathbf{x}=\mathbf{x}_{p,i}} + \boldsymbol{f}_{d,i}$, where $\mathcal{V}_{p,i}$ is the particle volume and $\boldsymbol{f}_{d,i}$ is the drag force calculated by the Wen and Yu (1966) drag law. The gas phase deviatoric stress tensor contribution is relatively insignificant in $\boldsymbol{f}_{g\rightarrow p,i}$ for modeling gas-fluidized beds of particles (Agrawal et al., 2001) and hence ignored. The total interaction force is mapped on the Eulerian grid using a mollification kernel ξ characterized by a smoothing length equal to the mesh spacing Δ by following Pepiot and Desjardins (2012). The kernel function ξ is defined by

$$\xi(\mathcal{L}) = \begin{cases} \frac{1}{4}\mathcal{L}^4 - \frac{5}{8}\mathcal{L}^2 + \frac{115}{192}, & \text{if } \mathcal{L} \leq 0.5 \\ -\frac{1}{6}\mathcal{L}^4 + \frac{5}{6}\mathcal{L}^3 - \frac{5}{4}\mathcal{L}^2 + \frac{5}{24}\mathcal{L} + \frac{55}{96}, & \text{if } 0.5 < \mathcal{L} \leq 1.5 \\ \frac{(2.5-\mathcal{L})^4}{24}, & \text{if } 1.5 < \mathcal{L} \leq 2.5 \\ 0, & \text{otherwise} \end{cases} \tag{10}$$

where $\mathcal{L} = d/\Delta$ and d is the distance from the particle position $\mathbf{x}_{p,i}$ to face center coordinate $\mathbf{x}$. The total force is mapped over the 27 nearest cells around the particle location. Alternatively, the mapping of Lagrangian properties on the Eulerian mesh could be performed by using trilinear interpolation (Snider et al., 1998; Patankar and Joseph, 2001). Subscript i indicates that quantities are per particle, and that fluid phase properties have been interpolated at the particle position, $|_{\mathbf{x}=\mathbf{x}_{p,i}}$. The fluid variables at the particle position are computed by a linear interpolation using the distance weightings $\mathcal{L}$.

The gas phase equations are solved using an OpenFOAM-based Computational Fluid Dynamics solver (OpenFOAM, 2013), while the particle phase DEM equations are evolved via the LIGGGHTS platform (Kloss et al., 2011). The two phases are coupled via CFDEMcoupling (Kloss et al., 2012; Goniva et al., 2012).

We performed simulations in periodic domains in which one can examine the flow dynamics without wall-induced restrictions. To drive the flow in this periodic domain, we decompose the pressure term p_g in Eq. (9) into two components as follows: $p_g(\boldsymbol{x},t) = p_g''(\boldsymbol{x},t) - \bar{\rho}||\boldsymbol{g}||(z-z_o)$. Here, p_g'' is the computed gas pressure that obeys the periodic boundary condition and $\bar{\rho}||\boldsymbol{g}||(z-z_o)$ represents the mean vertical pressure drop due to the total mass of a two-phase mixture; $\bar{\rho}$ is the domain-averaged mixture density; z is the coordinate in the direction that is opposite of gravity and z_o is a reference elevation.

Although we will present our results in dimensionless form, it is useful to present typical dimensional quantities to demonstrate that the simulations have been done for gas-particle systems of practical interest. With this in mind, we present the simulation parameters in both dimensional and dimensionless forms in Table 1. Simulations were performed for three different domain-averaged solid volume fractions $< \phi >$: 0.02, 0.1, 0.2 and 0.3, and three different particle sizes. The simulations were run for a sufficiently long

Figure 2: Snapshots of the particle volume fraction field in a periodic domain. Simulations' parameters are listed in Table 1. Domain-averaged particle volume fraction $< \phi >$ is (a) 0.02, (b) 0.1 and (c) 0.3. The gray scale axis ranges from 0 (white) to 0.64 (black). Particle Froude number is 88.4.

duration ($10\,\tau_p^{St}$) to ensure that a statistical steady state is reached (see Table 1 for the definition of τ_p^{St}). Subsequently, snapshots were collected at every τ_p^{St} time instant for a duration of $20\,\tau_p^{St}$. Snapshots of the particle volume fraction fields obtained in simulations with different domain-averaged solid volume fraction are shown in Figure 2, for particles with a diameter of $75\,\mu m$. The computational data from these snapshots were then filtered, binned in terms of filtered volume fraction and filter size.

Table 1: Computational domain and simulations parameters.

Simulations Parameters	**Value**
Particle diameter; d_p $[\mu m]$	75 / 150 / 300
Domain size; $(d_p \times d_p \times d_p)$	$240 \times 240 \times 960$
Grid size; $(d_p \times d_p \times d_p)$	$3 \times 3 \times 3$
Acceleration due to gravity; $\mathbf{g}$ $[m/s^2]$	9.81
Particle density; ρ_p $[kg/m^3]$	1500
Young's modulus; Y $[Pa]$	10^6
Poisson's ratio; ν	0.42
Restitution coefficient; e	0.9
Particle-particle friction coefficient; μ_p	0.5
Gas density; ρ_g $[kg/m^3]$	1.3
Gas viscosity; μ_g $[Pa \cdot s]$	1.8×10^{-5}
Stokes relaxation time; $\tau_p^{St} = \frac{\rho_p {d_p}^2}{18\mu_g}$ $[s]$	0.026 / 0.104 / 0.416
Terminal velocity of a single particle based on Wen and Yu (1966) drag law; v_t $[m/s]$	0.255 / 1.022 / 4.080
Domain-averaged solid volume fraction $< \phi >$	0.02 / 0.1 / 0.2† / 0.3‡
Number of particles	$2.1 \times 10^6/10.5 \times 10^6/21 \times 10^6/31.5 \times 10^6$
Froude number based on terminal velocity; $Fr_p = {v_t}^2/(\|\|\mathbf{g}\|\|d_p)$	88.4 / 709.8 / 5656.3

† The simulations with the domain-averaged solid volume fraction of 0.2 were performed only for particles with diameters of $150\,\mu m$ and $300\,\mu m$.

‡ The simulation with the domain-averaged solid volume fraction of 0.3 was performed only for particles with a diameter of $75\,\mu m$.

3. Coarsening Procedure

3.1. Fluid Coarsening

The correction to the drag force needed for Euler-Lagrange simulations with coarser fluid grids was deduced by filtering the results from highly resolved simulations. Firstly, the particle volume fraction, gas pressure and gas velocity were filtered using various filter sizes Δ_f around each computational node. The filtered solid volume fraction is computed by

$$\overline{\phi}(\mathbf{x}, t) = \int\int\int \phi(\mathbf{r}, t) G(\mathbf{r} - \mathbf{x}) d\mathbf{r} \tag{11}$$

where $G(\mathbf{r}-\mathbf{x})$ is a weight function which satisfies $\int\int\int\ G(\mathbf{r})d\mathbf{r}=1$. The box filter kernel is given by

$$G(\mathbf{r}-\mathbf{x})=\begin{cases}\frac{1}{\Delta_f^3}, & \text{if } |\mathbf{r}-\mathbf{x}|\leq\frac{\Delta_f}{2}\\ 0, & \text{otherwise}\end{cases} \tag{12}$$

The filtered gas velocity is defined as

$$\tilde{u}_g(\mathbf{x},t)=\frac{1}{(1-\overline{\phi})}\int\int\int\ G(\mathbf{r}-\mathbf{x})(1-\phi(\mathbf{r},t))u_g(\mathbf{r},t)d\mathbf{r}. \tag{13}$$

The filtered gas pressure is

$$\overline{p}_g(\mathbf{x},t)=\int\int\int\ G(\mathbf{r}-\mathbf{x})p_g(\mathbf{r},t)d\mathbf{r}. \tag{14}$$

They were then interpolated to each particle location to compute the filtered Lagrangian drag coefficient on each particle as follows:

$$\overline{\beta}_{i,\alpha}^{Lag} = \frac{1}{(\tilde{u}_{g,\alpha}|_{\mathbf{x}=\mathbf{x}_{p,i}}-v_{i,\alpha})}\Big[-\mathcal{V}_{p,i}\boldsymbol{\nabla}_\alpha\, p_g|_{\mathbf{x}=\mathbf{x}_{p,i}}+\mathcal{V}_{p,i}\boldsymbol{\nabla}_\alpha\,\overline{p}_g|_{\mathbf{x}=\mathbf{x}_{p,i}}+\beta_i^{Lag}(u_{g,\alpha}|_{\mathbf{x}=\mathbf{x}_{p,i}}-v_{i,\alpha})\Big] \tag{15}$$

where α is the direction, x, y, z, ∇_α is the gradient in the direction of α, $v_{i,\alpha}$ is the α component of the particle velocity and β_i^{Lag} is the drag coefficient (Wen and Yu (1966) law used in highly resolved simulations) evaluated at the solid volume fraction and the slip velocity at the particle location. Since the sub-grid contribution of gas pressure gradient is found to be small (Igci et al., 2008; Ozel et al., 2013), we introduced that contribution into the filtered drag coefficient, (in Eq. (15)) instead of proposing a separate model.

3.2. Particle Coarsening

We visualize a parcel as a particle that is a representative for a prescribed number of real particles. In this case, the filtered drag force according to which the parcels interact with fluid should reflect the effect of fine-scale particle structure lost through the particle coarsening. Parcels were created from the highly resolved CFD-DEM snapshots in the following manner. The analysis begins with prescribed number of particles n_p in a parcel, and a desired fluid filter size as in fluid coarsening. Then for each particle in a snapshot, its n_p-1 closest neighbors were identified; the location and velocity of a parcel representing a collection of these n_p particles and the fluid-particle force acting on this parcel were then found using those for the individual particles. Using these parcel quantities and the fluid-coarsened information interpolated to the parcel location, the correction to the drag coefficient was deduced. The filtered parcel drag coefficient based on *a priori* construction is given by

$$\begin{aligned}\overline{\beta}_{i,\alpha}^{par} = & \frac{1}{(\tilde{u}_{g,\alpha}|_{\mathbf{x}=\mathbf{x}_{par,i}}-\frac{1}{n_p}\sum_{j=1}^{n_p}u_{j,\alpha})}\\ & \Big[\mathcal{V}_{par,i}\nabla_\alpha\,\tilde{p}_g|_{\mathbf{x}=\mathbf{x}_{par,i}}-\sum_{j=1}^{n_p}\mathcal{V}_{p,j}\nabla_\alpha\,p_g|_{\mathbf{x}=\mathbf{x}_{p,j}}+\sum_{j=1}^{n_p}\beta_j^{Lag}(u_{g,\alpha}|_{\mathbf{x}=\mathbf{x}_{p,j}}-v_\alpha)\Big]/n_p\end{aligned} \tag{16}$$

where $|_{\mathbf{x}=\mathbf{x}_{par,i}}$ denotes the filtered gas variables at the parcel location and $\mathcal{V}_{par,i}$ is the parcel volume that equals to the total volume of the particles participating in a parcel, $n_p\mathcal{V}_p$. It is then divided by n_p (i.e. expressed on a per particle basis) so that one can compare $\overline{\beta}^{par}$ and $\overline{\beta}^{Lag}$.

3.3. Euler-Euler filtering

One of the goals of this study is to assess the difference between filtered Euler-Euler and Euler-Lagrange results. We can use this analysis to argue if one can use Euler-Euler filtered drag model in MP-PIC simulations or vice-versa. To perform Euler-Euler filtering, we first mapped the solid velocity u_s to the cell centers in *a priori* manner by using the mollification kernel given in Eq. (10). Then, we computed the filtered Eulerian drag coefficient as:

$$\overline{\beta}^{Eul}_{\alpha} = \frac{1}{(\tilde{u}_{g,\alpha} - \tilde{u}_{s,\alpha})}\left[\overline{\phi}\nabla_\alpha \overline{p}_g - \overline{\phi\nabla_\alpha p_g} + \overline{\beta^{Eul}(u_{g,\alpha} - u_{s,\alpha})}\right]$$

where $\tilde{u}_{s,\alpha}$ is the filtered solid velocity at the cell center and given by

$$\tilde{u}_s(\mathbf{x},t) = \frac{1}{\overline{\phi}}\int\int\int G(\mathbf{r}-\mathbf{x})\phi(\mathbf{r},t)u_s(\mathbf{r},t)d\mathbf{r} \tag{17}$$

and β_i^{Eul} is the Eulerian drag coefficient (Wen and Yu (1966)).

4. Filtering Results

The filtered Eulerian drag coefficient as a function of the filtered particle volume fraction for various filter sizes is shown in Figure 3. It reveals a significant reduction in filtered drag coefficient even when the filter size is only $9\,d_p$. This means that when we perform TFM simulations, a sub-grid correction to the drag law is necessary even with grid sizes as small as $9\,d_p$. This could be one reason why TFM simulations show grid size sensitivity even with very fine grids , and in case a filtered drag model is not used.

The filtered Lagrangian drag coefficient as a function of the filtered particle volume fraction for various filter sizes is shown in Figure 4. Here, only fluid coarsening has been performed, as was done by Radl and Sundaresan (2014); the present analysis considers much larger filter sizes. The strong effect of fluid filter size seen in Figure 4.

The outcome of particle coarsening is presented in Figure 5a and 5b for particles with $Fr_p = 88.4$. The filtered parcel drag correction is presented in these figures as a function of filtered particle volume fraction for various parcel sizes and two different filter sizes. The figures also include the filtered Eulerian drag correction. The filtered parcel drag correction changes slightly upon increasing the parcel size from 1 to 8 particles, but any further increase produces little change. The filtered parcel drag correction for parcel sizes of 8 or larger is close to the filtered Eulerian drag correction at most filtered particle volume fraction. It is readily apparent from Figures 4 and 6 that correction to the filtered drag coefficient comes largely from fluid coarsening.

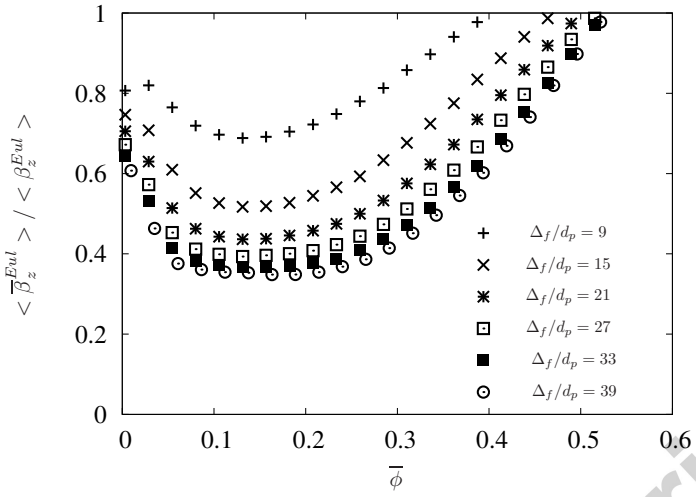

Figure 3: Normalized filtered Eulerian drag coefficient as a function of the filtered particle volume fraction for various filter sizes. Froude number is 88.4. The reference drag coefficient in the normalization is based on the filtered slip velocity and the filtered particle volume fraction. Physical properties of gas are summarized in Table 1.

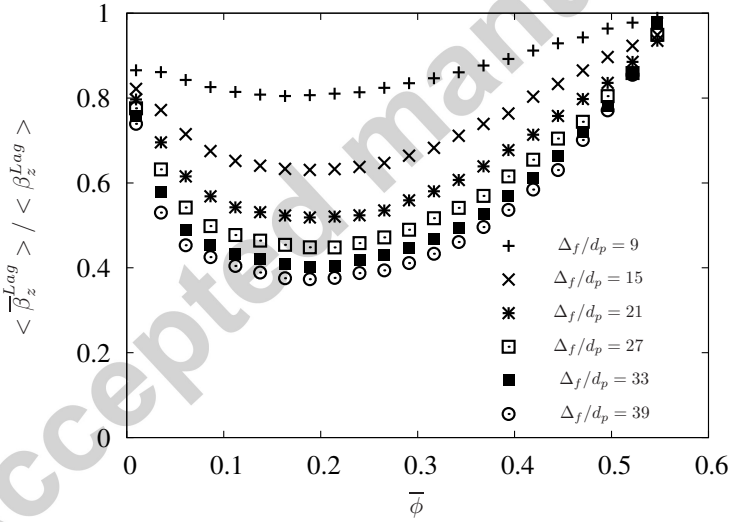

Figure 4: Normalized filtered Lagrangian drag coefficient as a function of the filtered particle volume fraction for various filter sizes. Froude number is 88.4. Physical properties of gas are summarized in Table 1.

Radl and Sundaresan (2014) did not perform a particle-coarsening analysis, but carried out *a posteriori* tests of coarse CFD-DPM model. Towards this end, they compared the domain-averaged slip velocity in a periodic domain obtained through the reference CFD-DEM and coarse CFD-DPM simulations. They found that when coarse drag coefficient generated only through fluid coarsening was employed, the difference between the domain-averaged slip velocities of coarse CFD-DPM and reference CFD-DEM simulation increased with parcel size, n_p. This led them to speculate that the filtered drag correction is dependent on the particle coarsening as well. The present particle-coarsening analysis shows clearly that this speculation

is incorrect and that the origin of the difference is elsewhere. In coarse CFD-DPM simulations, collisions between parcels (which are treated as pseudo-particles of diameter $n^{1/3}d_p$ and same density as the original particles) are tracked. Our particle-coarsening results show that the idealizations that went into parcel-parcel interactions (and not particle-coarsening of drag law) is the source of discrepancy.

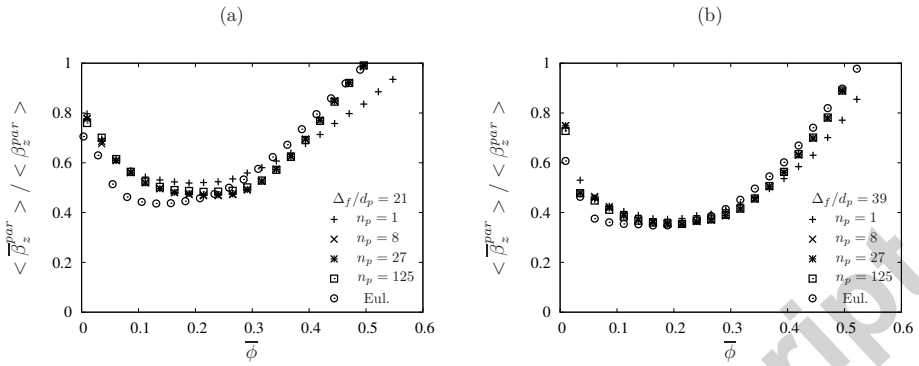

Figure 5: Normalized filtered parcel drag coefficient as a function of the filtered particle volume fraction for various number of particles in a parcel. The filter sizes Δ_f are equal to $21\,d_p$ (left) and $39\,d_p$ (right). Froude number is 88.4. Normalized filtered Eulerian drag coefficient for the filter size equal to $21\,d_p$ (left) and $39\,d_p$ (right) is also plotted. Physical properties of gas are summarized in Table 1.

Figure 6a and 6b present the filtered parcel drag correction as a function of filtered particle volume fraction for two other particle sizes (equivalently, particle Froude numbers). The results are shown for parcel sizes of 27 and 125, and a filter size of $39d_p$. The negligible effect of particle coarsening persists for the larger particles as well. Also shown in these figures are the filtered Eulerian drag corrections. The correlation of Schneiderbauer and Pirker (2014) is also plotted in Figure 6a. Once again, the Eulerian and Lagrangian drag corrections are quite similar in magnitude; in general, the Lagrangian drag coefficient is somewhat larger (smaller) than the Eulerian one at small (large) filtered particle volume fractions. These could be due to the fact that the Lagrangian drag coefficient is evaluated at the parcel position, while the Eulerian quantity is evaluated at the fluid cell center. Irrespective of this distinction, it is clear from Figures 5 and 6 that at volume fractions typical of turbulent fluidized beds, coarse MP-PIC and CFD-DPM simulations would require drag corrections comparable to that required by coarse TFM simulations.

The results presented for the $75\,\mu m$ particles were obtained from simulations with domain-average volume fraction of 0.02, 0.1 and 0.3. Simulations for the two larger particles with domain-averaged volume fraction of 0.3 formed nearly one-dimensional, vertically traveling particle plugs, revealing that one would need even larger simulation domains to capture three-dimensional structures. At this domain-average volume fractions, our simulations already involved > 30 million particles and required more than 150 hours of computations on 256 cores; at the present time, anything larger is beyond available resources. Simulations with $< \phi >= 0.2$ for these two particle sizes were found to yield three-dimensional structures (in this simulation domain); as a result, the results shown for the two larger particle sizes represent averages extracted from simulations with domain-average volume fraction of 0.02, 0.1 and 0.2.

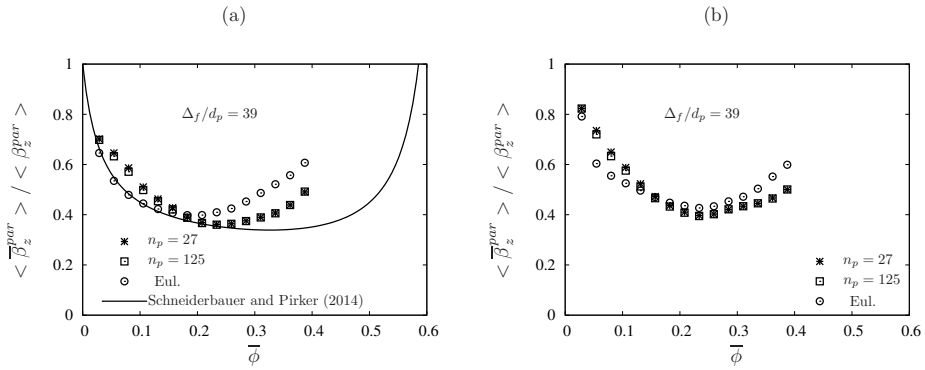

Figure 6: Normalized filtered parcel drag coefficient as a function of the filtered particle volume fraction for various number of particles in a parcel. The filter size Δ_f is equal to $39\,d_p$. Froude numbers are 709.8 (left) and 5656.3 (right). Normalized filtered Eulerian drag coefficient for the filter size equal to $39\,d_p$ is also plotted. The function proposed by Schneiderbauer and Pirker (2014) is also plotted. The dimensionless gas velocity (Schneiderbauer and Pirker (2014)'s Eq.23, pp 884) is set to 1. Domain-averaged solid volume fractions are equal to 0.02, 0.1 and 0.2. Physical properties of gas and particles used in the simulations are summarized in Table 1.

Earlier studies on correction to Eulerian drag coefficient, extracted from highly resolved TFM simulations, have sought to correlate the correction to the filtered drag coefficient in terms of filter size and filtered particle volume fraction (Igci and Sundaresan, 2011a; Parmentier et al., 2012) as

$$\frac{< \overline{\beta}^{Eul} >}{< \beta^{Eul} >} = 1 - H(\Delta_f, \overline{\phi}). \tag{18}$$

Igci and Sundaresan (2011a) and Parmentier et al. (2012) scaled the filter size differently. Igci and Sundaresan (2011a) proposed

$$H = \frac{Fr_f^{-1/3}}{1.5 + Fr_f^{-1/3}} h_{2D}(\overline{\phi}), \qquad Fr_f = \frac{||\mathbf{g}||\Delta_f}{v_t^2}, \tag{19}$$

while Parmentier et al. (2012) wrote:

$$H = \frac{\Delta_f^{*2}}{0.0613 + \Delta_f^{*2}} H_\infty(\overline{\phi}), \qquad \Delta_f^* = \frac{\Delta_f \tau_p^{St}}{\sqrt{||\mathbf{g}|| D_H}} \tag{20}$$

Here, D_H is the hydraulic diameter of the bed. Note that in the above correlations, H approaches to $h_{2D}(\overline{\phi})$ (Igci and Sundaresan, 2011a) or $H_\infty(\overline{\phi})$ (Parmentier et al., 2012), at the limit of very large filter sizes. While Igci and Sundaresan (2011a) presented an explicit correlation for $h_{2D}(\overline{\phi})$, which is not reproduced here, Parmentier et al. (2012) argued that $H_\infty(\overline{\phi})$ can only be found to within a multiplicative constant κ which depends on the simulated case and is dynamically adjusted in the coarse simulations: $H_\infty(\overline{\phi}) = \kappa h(\overline{\phi})$ where

$$h(\overline{\phi}) = \sqrt{\frac{\overline{\phi}}{\phi_{max}}} \left(1 - \frac{\overline{\phi}}{\phi_{max}}\right) \left[1 - 1.88\frac{\overline{\phi}}{\phi_{max}} + 5.16\left(\frac{\overline{\phi}}{\phi_{max}}\right)^2\right]. \tag{21}$$

Their analyses suggested that κ will be in the range of $2 - 4$.

In the present study, we estimated this asymptotic limit as follows. The filtered Eulerian drag correction is first plotted against the inverse of filter size for various values of $\overline{\phi}$, as illustrated in Figure 7, where a nearly linear dependence is readily apparent for the three largest filter sizes. Accordingly, the data for the three largest filter sizes were fit to a straight line and extrapolated to very large filter sizes. Needless to say that such extrapolation is not reliable; however, it is a convenient way of generating a compact correlation that can be applied within the range of filter sizes for which filtered results are generated. The y-intercepts for various $\overline{\phi}$ values obtained through such an analysis for the particles with $Fr_p = 88.4$ are presented in Figure 8. Such extrapolation was done for both Eulerian and Lagrangian corrections. The figure also shows $h_{2D}(\overline{\phi})$ of Igci and Sundaresan (2011a) and $H_\infty(\overline{\phi})$ of Parmentier et al. (2012). While plotting $H_\infty(\overline{\phi})$, we set $\phi_{max} = 0.587$ for particles with friction coefficient of 0.5 used in our simulations (motivated by the results of Chialvo et al. (2012) for the critical particle concentration in granular shear flows) and adjusted κ to get a good fit ($\kappa = 3.1$).

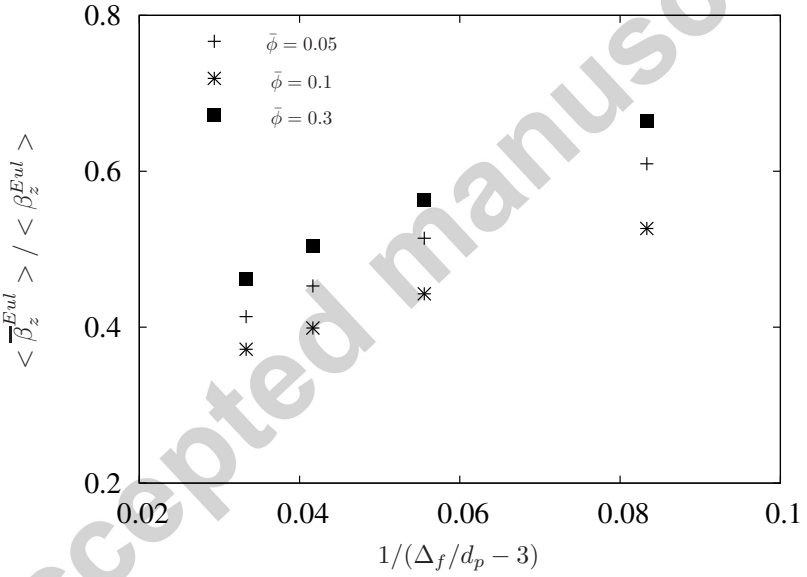

Figure 7: Normalized filtered Eulerian drag coefficient as a function of the inverse filter length at three filtered solid volume fractions, $\bar{\phi} = 0.05$, 0.1 and 0.3. Froude numbers is 88.4. Physical properties of gas and particles used in the simulations are summarized in Table 1.

Figure 8 clarifies two points. First, filtering the same data set leads to similar correction to the drag law for both filtered TFM and MP-PIC approaches. Small quantitative differences found in the drag corrections to be deployed in filtered TFM and MP-PIC (or CFD-DPM) simulations could indeed be due to the differences in the location where the drag law is applied: drag force is evaluated at the Eulerian grid in the case of TFM, while it is found at the particle (parcel) location in CFD-DPM and MP-PIC simulations. However, this difference is only modest, except at very low volume fractions. Second, the shape of the correction function deduced in the present study based on snapshots generated through CFD-DEM data is very similar to those found in earlier studies employing finely resolved TFM simulations to deduce the correction. This

reassures as it indicates robustness of the corrections.

The asymptotic limit deduced by Igci and Sundaresan (2011a) does not allow for dynamic adjustment, while that due to Parmentier et al. (2012) does. The superior fit seen with the latter model is due to this adjustable parameter. Parmentier et al. (2012) have also presented an elegant approach to deduce the value of this adjustable parameter in coarse simulations. Figure 8 suggests that it would be good to include such dynamic adjustment of drag coefficient in simulations of filtered TFM, CFD-DPM and MP-PIC simulations.

Figure 9a shows the asymptotic limit to the Eulerian drag correction for the three different particle sizes. As noted earlier, simulations manifesting three-dimensional structures formed for the larger particles only when the domain-averaged volume fraction was small. As a result, we could generate through CFD-DEM approach the drag correction only for a limited volume fraction range for the two larger particle sizes explored. Figure 9b shows analogous Lagrangian corrections. It is clear from these figures that the asymptotic limit depends on particle Froude number, which has not been examined carefully in previous studies. By allowing κ to be different for systems with different Froude numbers, as illustrated in 9a, one could partly capture the effect of Froude number on drag correction. As noted earlier, in the correction proposed by Parmentier et al. (2012) κ is determined dynamically in coarse-grid simulations; whether such a dynamic model will capture the Froude number effect remains to be tested in future studies.

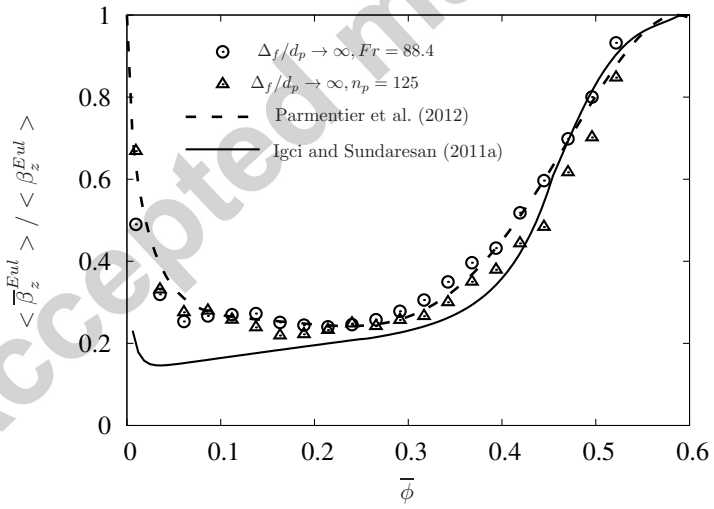

Figure 8: Normalized filtered Eulerian and parcel drag coefficients as a function of the filtered particle volume fraction at the limit of the infinite filter size. Number of particles in a parcel was set to 125. The functions proposed by Parmentier et al. (2012) and Igci and Sundaresan (2011b) are also plotted. The constant of Parmentier et al. (2012)'s model is 3.1. ϕ_{max} is equal to 0.587. Physical properties of gas are summarized in Table 1.

5. Summary

We have performed CFD-DEM simulations of gas-fluidization of particles in periodic domains at volume fractions typically observed in circulating fluidized beds and turbulent fluidized beds. We then asked how

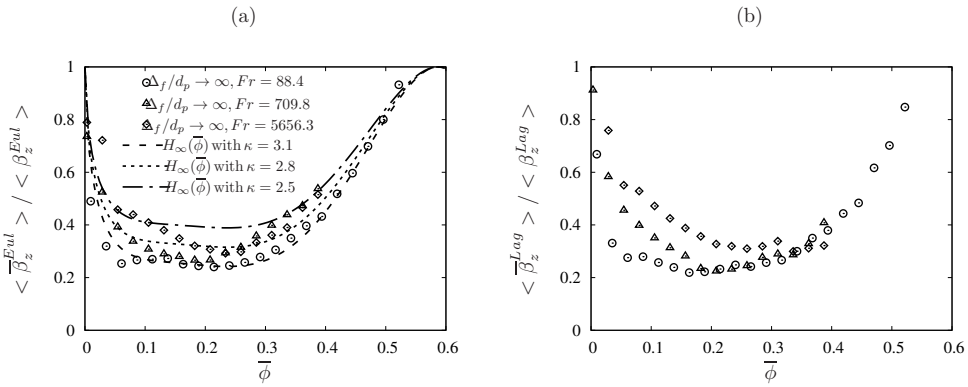

Figure 9: Normalized filtered Eulerian (left) and parcel (right) drag coefficients as a function of the filtered particle volume fraction at the limit of the infinite filter size. Froude numbers are 88.4, 709.8 and 5656.3. The function proposed by Parmentier et al. (2012) is also plotted. The constants of Parmentier et al. (2012)'s model are 3.1, 2.8 and 2.5 for Froude numbers of 88.4, 709.8 and 5656.3, respectively. ϕ_{max} is equal to 0.587. Physical properties of gas are summarized in Table 1.

one should systematically coarse-grain these results to deduce the effective drag model for coarse CFD-DPM or MP-PIC simulations and the filtered TFM approach. We demonstrate that the filtered Lagrangian drag coefficient decreases upon coarsening the fluid grid. Particle coarsening has a weaker effect when compared to fluid coarsening.

We have also mapped the Lagrangian quantities to the Eulerian grid and computed the filtered Eulerian drag coefficients. The drag corrections to be deployed in filtered TFM and MP-PIC (or CFD-DPM) simulations are found to be comparable. Therefore, one can use, at least as a good first approximation, the drag corrections deduced for filtered TFM simulations in coarse MP-PIC and CFD-DPM simulations and vice versa.

The asymptotic limit of the drag correction applicable to large filter sizes deduced in the present study (for the $75\mu m$ particles fluidized by ambient air) based on CFD-DEM simulations is comparable to that found in earlier studies through finely resolved TFM simulations. This demonstrates the robustness of the corrections. As shown recently by Fullmer and Hrenya (2016), finely resolved Euler-Euler simulations based on KTGF performed in periodic domains agree qualitatively and nearly quantitatively (to within 20%) with analogous CFD-DEM simulations. Therefore, it is not surprising that the corrections to the drag law obtained in the present study based on CFD-DEM simulations are close to those generated through finely resolved Euler-Euler models (Igci and Sundaresan, 2011b; Parmentier et al., 2012). These reinforce the notion that these corrections are robust and not sensitive to modeling approach. In dense fluidized beds, frictional stresses, not considered in KTGF, could come into play; recent studies by Cloete et al. (2016) and Schneiderbauer and Pirker (2016) found that frictional stress did not lead to appreciable change in the drag correction. Also, Cloete et al. (2016) have recently supported the argument that the exact functional form of the drag law has only a little effect on the corrections accounting for particle clustering.

Furthermore, the presented methodology could be used to formulate coarse models for systems manifesting multi-physics such as cohesion introduced through liquid bridges between particles, cohesion or repulsion

due to electrostatic charges carried by the particles and cohesion through van der Waals interaction. However, it still needs to be firmly established if the findings presented in our current contribution can be transferred directly to cohesive particulate systems.

In the present study, the drag correction for each gas-particle system is expressed as a function of filter size and filtered particle volume fraction. Some earlier studies (Milioli et al. (2013); Schneiderbauer et al. (2013); Ozel et al. (2013)) focusing on drag models for filtered TFM found that the drag correction should include additional markers such as local filtered slip velocity. We have not explored such complexities in the present study. It would be interesting to explore whether additional local markers such as filtered slip velocity or non-local information such gradients of filtered solid volume fraction and velocities, would improve quantitative predictions of filtered models.

It would be of interest to analyze CFD-DEM results to formulate filtered stress models and demonstrate that they are similar to those found by analyzing TFM results. One can then confidently use the CFD-DEM approach to develop coarse-grained stress models for systems with complex particle-particle interactions for which constitutive models needed in TFM are not available.

Acknowledgement

This study was supported by ExxonMobil Research & Engineering Company.

Agrawal, K., Loezos, P.N., Syamlal, M., Sundaresan, S., 2001. The role of meso-scale structures in rapid gas-solid flows. Journal of Fluid Mechanics 445, 151–185.

Balzer, G., Boelle, A., Simonin, O., 1998. Eulerian gas-solid flow modelling of dense fluidized bed, in: Fluidization VIII – International symposium of Engineering Foundation, pp. 1125–1134.

Benyahia, S., Sundaresan, S., 2012. Do we need sub-grid scale corrections for both continuum and discrete gas-particle flow models? Powder Technology 220, 2–6.

Capecelatro, J., Desjardins, O., 2013. An EulerLagrange strategy for simulating particle-laden flows. Journal of Computational Physics 238, 1–31.

Capecelatro, J., Desjardins, O., Fox, R.O., 2014a. Numerical study of collisional particle dynamics in cluster-induced turbulence. Journal of Fluid Mechanics 747, R2.

Capecelatro, J., Desjardins, O., Fox, R.O., 2016a. Strongly coupled fluid-particle flows in vertical channels. I. Reynolds-averaged two-phase turbulence statistics. Physics of Fluids (1994-present) 28, 033306.

Capecelatro, J., Desjardins, O., Fox, R.O., 2016b. Strongly coupled fluid-particle flows in vertical channels. II. Turbulence modeling. Physics of Fluids (1994-present) 28, 033307.

Capecelatro, J., Pepiot, P., Desjardins, O., 2014b. Numerical characterization and modeling of particle clustering in wall-bounded vertical risers. Chemical Engineering Journal 245, 295–310.

Chialvo, S., Sun, J., Sundaresan, S., 2012. Bridging the rheology of granular flows in three regimes. Physical Review E 85, 021305.

Cloete, J.H., Cloete, S., Municchi, F., Radl, S., Amini, S., 2016. The sensitivity of filtered Two Fluid Models to the underlying resolved simulation setup, in: Fluidization XV – International symposium of Engineering Foundation.

Cundall, P.A., Strack, O.D.L., 1979. A discrete numerical model for granular assemblies. Gotechnique 29, 47–65.

Derksen, J.J., Sundaresan, S., 2007. Direct numerical simulations of dense suspensions: wave instabilities in liquid-fluidized beds. Journal of Fluid Mechanics 587, 303–336.

Di Renzo, A., Di Maio, F.P., 2004. Comparison of contact-force models for the simulation of collisions in DEM-based granular flow codes. Chemical Engineering Science 59, 525–541.

Ding, J., Gidaspow, D., 1990. A bubbling fluidization model using kinetic theory of granular flow. AIChE Journal 36, 523–538.

Fede, P., Simonin, O., 2006. Numerical study of the subgrid fluid turbulence effects on the statistics of heavy colliding particles. Physics of Fluids (1994-present) 18, 045103.

Fox, R.O., 2014. On multiphase turbulence models for collisional fluidparticle flows. Journal of Fluid Mechanics 742, 368–424.

Fries, L., Antonyuk, S., Heinrich, S., Dopfer, D., Palzer, S., 2013. Collision dynamics in fluidised bed granulators: A DEM-CFD study. Chemical Engineering Science 86, 108–123.

Fullmer, W.D., Hrenya, C.M., 2016. Quantitative assessment of fine-grid kinetic-theory-based predictions of mean-slip in unbounded fluidization. AIChE Journal 62, 11–17.

Gidaspow, D., 1994. Multiphase Flow and Fluidization: Continuum and Kinetic Theory Descriptions. 1 edition ed., Academic Press, Boston.

Girardi, M., Radl, S., Sundaresan, S., 2016. Simulating wet gassolid fluidized beds using coarse-grid CFD-DEM. Chemical Engineering Science 144, 224–238.

Goniva, C., Kloss, C., Deen, N.G., Kuipers, J.A.M., Pirker, S., 2012. Influence of rolling friction on single spout fluidized bed simulation. Particuology 10, 582–591.

Gu, Y., Ozel, A., Sundaresan, S., 2016. Numerical studies of the effects of fines on fluidization. AIChE Journal 62, 2271–2281.

Igci, Y., Andrews, A.T., Sundaresan, S., Pannala, S., O'Brien, T., 2008. Filtered two-fluid models for fluidized gas-particle suspensions. AIChE Journal 54, 1431–1448.

Igci, Y., Sundaresan, S., 2011a. Constitutive Models for Filtered Two-Fluid Models of Fluidized GasParticle Flows. Industrial & Engineering Chemistry Research 50, 13190–13201.

Igci, Y., Sundaresan, S., 2011b. Verification of filtered two-fluid models for gas-particle flows in risers. AIChE Journal 57, 2691–2707.

Jackson, R., 2000. The Dynamics of Fluidized Particles. Cambridge University Press.

Johnson, K.L., Johnson, K.L., 1987. Contact Mechanics. Cambridge University Press.

Kaufmann, A., Moreau, M., Simonin, O., Helie, J., 2008. Comparison between Lagrangian and mesoscopic Eulerian modelling approaches for inertial particles suspended in decaying isotropic turbulence. Journal of Computational Physics 227, 6448–6472.

Kloss, C., Goniva, C., Hager, A., Amberger, S., Pirker, S., 2012. Models, algorithms and validation for opensource DEM and CFDDEM. Progress in Computational Fluid Dynamics, an International Journal 12, 140–152.

Kloss, C., Goniva, C., The Minerals, M..M.S.T., 2011. LIGGGHTS Open Source Discrete Element Simulations of Granular Materials Based on Lammps, in: Supplemental Proceedings. John Wiley & Sons, Inc., pp. 781–788.

Kobayashi, T., Tanaka, T., Shimada, N., Kawaguchi, T., 2013. DEMCFD analysis of fluidization behavior of Geldart Group A particles using a dynamic adhesion force model. Powder Technology 248, 143–152.

Koch, D.L., Ladd, A.J.C., 1997. Moderate Reynolds number flows through periodic and random arrays of aligned cylinders. Journal of Fluid Mechanics 349, 31–66.

Koch, D.L., Sangani, A.S., 1999. Particle pressure and marginal stability limits for a homogeneous monodisperse gas-fluidized bed: kinetic theory and numerical simulations. Journal of Fluid Mechanics 400, 229–263.

Kolehmainen, J., Ozel, A., Boyce, C.M., Sundaresan, S., 2016. A hybrid approach to computing electrostatic forces in fluidized beds of charged particles. AIChE Journal .

Li, J., Kwauk, M., 1994. The Energy-Minimization Multi-Scale Method, Metallurgical Industry Press. Beijing, PR China .

Lun, C.K.K., Savage, S.B., Jeffrey, D.J., Chepurniy, N., 1984. Kinetic Theories for Granular Flow: Inelastic Particles in Couette Flow and Slightly Inelastic Particles in a General Flowfield. Journal of Fluid Mechanics 140, 223–256.

Milioli, C.C., Milioli, F.E., Holloway, W., Agrawal, K., Sundaresan, S., 2013. Filtered two-fluid models of fluidized gas-particle flows: New constitutive relations. AIChE Journal 59, 3265–3275.

Moreau, M., Simonin, O., Bdat, B., 2009. Development of Gas-Particle Euler-Euler LES Approach: A Priori Analysis of Particle Sub-Grid Models in Homogeneous Isotropic Turbulence. Flow, Turbulence and Combustion 84, 295–324.

O'Brien, T.J., 2014. A multiphase turbulence theory for gassolid flows: I. Continuity and momentum equations with Favre-averaging. Powder Technology 265, 83–87.

OpenFOAM, 2013. OpenFOAM 2.2.2, User Manual .

O'Rourke, P.J., Snider, D.M., 2012. Inclusion of collisional return-to-isotropy in the MP-PIC method. Chemical Engineering Science 80, 39–54.

O'Rourke, P.J., Zhao, P.P., Snider, D., 2009. A model for collisional exchange in gas/liquid/solid fluidized beds. Chemical Engineering Science 64, 1784–1797.

Ozarkar, S.S., Yan, X., Wang, S., Milioli, C.C., Milioli, F.E., Sundaresan, S., 2015. Validation of filtered two-fluid models for gas-particle flows against experimental data from bubbling fluidized bed. Powder Technology 284, 159–169.

Ozel, A., Fede, P., Simonin, O., 2013. Development of filtered EulerEuler two-phase model for circulating fluidised bed: High resolution simulation, formulation and a priori analyses. International Journal of Multiphase Flow 55, 43–63.

Ozel, A., Vincent, S., Masbernat, O., Estivalezes, J., Abbas, M., Brndle de Motta, J., Simonin, O., 2016. Particle resolved direct numerical simulation of a Liquid-Solid Fluidized Bed: Comparison with Experimental Data. submitted for publication .

Parmentier, J.F., Simonin, O., Delsart, O., 2012. A functional subgrid drift velocity model for filtered drag prediction in dense fluidized bed. AIChE Journal 58, 1084–1098.

Patankar, N.A., Joseph, D.D., 2001. Modeling and numerical simulation of particulate flows by the EulerianLagrangian approach. International Journal of Multiphase Flow 27, 1659–1684.

Pepiot, P., Desjardins, O., 2012. Numerical analysis of the dynamics of two- and three-dimensional fluidized bed reactors using an EulerLagrange approach. Powder Technology 220, 104–121.

Radl, S., Sundaresan, S., 2014. A drag model for filtered EulerLagrange simulations of clustered gasparticle suspensions. Chemical Engineering Science 117, 416–425.

Rubinstein, G.J., Derksen, J.J., Sundaresan, S., 2016. Lattice Boltzmann simulations of low-Reynolds-number flow past fluidized spheres: effect of Stokes number on drag force. Journal of Fluid Mechanics 788, 576–601.

Salikov, V., Antonyuk, S., Heinrich, S., Sutkar, V.S., Deen, N.G., Kuipers, J.A.M., 2015. Characterization and CFD-DEM modelling of a prismatic spouted bed. Powder Technology 270, Part B, 622–636.

Schneiderbauer, S., Pirker, S., 2014. Filtered and heterogeneity-based subgrid modifications for gas-solid drag and solid stresses in bubbling fluidized beds. AIChE Journal 60, 839–854.

Schneiderbauer, S., Pirker, S., 2016. The impact of different fine grid simulations on the sub-grid modification for gassolid drag, in: 9th International Conference on Multiphase Flow, International Conference on Multiphase Flow (ICMF): Firenze, Italy.

Schneiderbauer, S., Puttinger, S., Pirker, S., 2013. Comparative analysis of subgrid drag modifications for dense gas-particle flows in bubbling fluidized beds. AIChE Journal 59, 4077–4099.

Simonin, O., 1991. Prediction of the dispersed phase turbulence in particle-laden jets.

Snider, D., Banerjee, S., 2010. Heterogeneous gas chemistry in the CPFD EulerianLagrangian numerical scheme (ozone decomposition). Powder Technology 199, 100–106.

Snider, D.M., 2001. An Incompressible Three-Dimensional Multiphase Particle-in-Cell Model for Dense Particle Flows. Journal of Computational Physics 170, 523–549.

Snider, D.M., 2007. Three fundamental granular flow experiments and CPFD predictions. Powder Technology 176, 36–46.

Snider, D.M., Clark, S.M., O'Rourke, P.J., 2011. EulerianLagrangian method for three-dimensional thermal reacting flow with application to coal gasifiers. Chemical Engineering Science 66, 1285–1295.

Snider, D.M., ORourke, P.J., Andrews, M.J., 1998. Sediment flow in inclined vessels calculated using a multiphase particle-in-cell model for dense particle flows. International Journal of Multiphase Flow 24, 1359–1382.

Sundaresan, S., 2000. Modeling the hydrodynamics of multiphase flow reactors: Current status and challenges. AIChE Journal 46, 1102–1105.

Syamlal, M., Rogers, W., OBrien, T.J., 1993. MFIX documentation: Theory guide. National Energy Technology Laboratory, Department of Energy, Technical Note DOE/METC-95/1013 and NTIS/DE95000031 .

Tenneti, S., Garg, R., Hrenya, C.M., Fox, R.O., Subramaniam, S., 2010. Direct numerical simulation of gassolid suspensions at moderate Reynolds number: Quantifying the coupling between hydrodynamic forces and particle velocity fluctuations. Powder Technology 203, 57–69.

Tenneti, S., Garg, R., Subramaniam, S., 2011. Drag law for monodisperse gassolid systems using particle-resolved direct numerical simulation of flow past fixed assemblies of spheres. International Journal of Multiphase Flow 37, 1072–1092.

Vance, M.W., Squires, K.D., Simonin, O., 2006. Properties of the particle velocity field in gas-solid turbulent channel flow. Physics of Fluids (1994-present) 18, 063302.

Vincent, S., Brndle de Motta, J.C., Sarthou, A., Estivalezes, J.L., Simonin, O., Climent, E., 2014. A Lagrangian VOF tensorial penalty method for the DNS of resolved particle-laden flows. Journal of Computational Physics 256, 582–614.

Wang, J., Ge, W., Li, J., 2008. Eulerian simulation of heterogeneous gas-solid flows in CFB risers: EMMS-based sub-grid scale model with a revised cluster description. Chemical Engineering Science 63, 1553–1571.

Wang, W., Li, J., 2007. Simulation of gassolid two-phase flow by a multi-scale CFD approachof the EMMS model to the sub-grid level. Chemical Engineering Science 62, 208–231.

Wen, C., Yu, Y., 1966. Mechanics of fluidization. Chem. Eng. Prog. Symp. Ser. 62, 100.

Ye, M., van der Hoef, M.A., Kuipers, J.A.M., 2004. A numerical study of fluidization behavior of Geldart A particles using a discrete particle model. Powder Technology 139, 129–139.